

Jeffery Orbits with Noise Revisited

J. Talbot and C. Antoine

*Laboratoire de Physique Théorique de la Matière Condensée (UMR CNRS 7600),
Sorbonne Université, 4 Place Jussieu, 75252 Paris Cedex 05, France*

P. Claudin

*Physique et Mécanique des Milieux Hétérogènes, PMMH UMR 7636 CNRS,
ESPCI Paris, PSL Research University, Sorbonne Université,
Université Paris Cité, 7 quai St Bernard, 75005 Paris, France*

E. Somfai and T. Börzsönyi

*Institute for Solid State Physics and Optics, HUN-REN Wigner
Research Centre for Physics, P.O. Box 49, H-1525 Budapest, Hungary*

(Dated: March 12, 2024)

The behavior of non-spherical particles in a shear-flow is of significant practical and theoretical interest. These systems have been the object of numerous investigations since the pioneering work of Jeffery a century ago. His eponymous orbits describe the deterministic motion of an isolated, rod-like particle in a shear flow. Subsequently, the effect of adding noise was investigated. The theory has been applied to colloidal particles, macromolecules, anisometric granular particles and most recently to microswimmers, for example bacteria. We study the Jeffery orbits of elongated particles subject to noise using Langevin simulations and a Fokker-Planck equation. We extend the analytical solution for infinitely thin needles ($\beta = 1$) obtained by Doi and Edwards to particles with arbitrary shape factor ($0 \leq \beta \leq 1$) and validate the theory by comparing it with simulations. We examine the rotation of the particle around the vorticity axis and study the orientational order matrix. We use the latter to obtain scalar order parameters s and r describing nematic ordering and biaxiality from the orientational distribution function. The value of s (nematic ordering) increases monotonically with increasing Péclet number, while r (measure of biaxiality) displays a maximum value. From perturbation theory we obtain simple expressions that provide accurate descriptions at low noise (or large Péclet numbers). We also examine the orientational distribution in the v -grad v plane and in the perpendicular direction. Finally we present the solution of the Fokker-Planck equation for a strictly two-dimensional (2D) system. For the same noise amplitude the average rotation speed of the particle in 3D is larger than in 2D.

I. INTRODUCTION

Two years ago marked the one hundredth anniversary of G. B. Jeffery's landmark paper [1], "The motion of ellipsoidal particles immersed in a viscous fluid". By calculating the torque on the particle in an unbounded fluid subject to a linear shear flow (creeping flow, or zero Reynold's number), he obtained a deterministic description of its time-dependent orientation. The particle's axis of revolution executes one of an infinite, one parameter, family of periodic orbits characterized by an orbital constant. The distribution of orientations is anisotropic, i.e certain orientations are preferred over others and this anisotropy increases with increasing elongation. There is no orbit for which the particle ceases to rotate.

Even a century after its publication, Jeffery's work is still relevant to many current research fields for a deep understanding of the behavior of sheared elongated particles, including rheology of granular flows and suspensions [2–14], nanoparticles, e.g. silica micro-rods in channels [15–17], red blood cells [18], as well as self-assembly and systems of active particles such as microswimmers [19–27].

Many subsequent articles built on Jeffery's pioneering work. Bretherton [28] extended the theory to ar-

bitrary particles of revolution and later, triaxial ellipsoids [29–31], charged fibers [32], curved particles [33] and time-dependent orientational distributions [34] have been studied. Other work focused on how the effect of inertia [35, 36] or the shear-thinning character of the fluid [37] changes the nature of particle rotation. Also, an alternative derivation of the original equations has been given [38].

Of particular interest in the context of the present article are the efforts to understand the effect of perturbations induced by fluctuations of the surrounding fluid or interaction with other particles on the trajectories. In this situation, the particle no longer remains on a single Jeffery orbit. The addition of a rotary Brownian motion therefore leads to steady state which no longer depends on the initial orientation. Early contributions from Boeder [39], Peterlin [40] and Burgers [41] were the first to consider the effect of Brownian motion on Jeffery orbits. Years later Leal and Hinch [42, 43] derived approximate expressions for the steady state distribution of orbital constants for weak and intermediate Brownian motion and applied the results to examine the rheological properties of suspensions of non-spherical particles.

In a landmark study, Doi and Edwards [44] developed a theory of rod-like macromolecules in concentrated so-

and

$$\begin{aligned}\frac{d\phi}{dt} &= -\dot{\gamma} \left(\frac{1+\beta}{2} \sin^2 \phi + \frac{1-\beta}{2} \cos^2 \phi \right) \\ &= -\frac{\dot{\gamma}}{2} (1 - \beta \cos(2\phi)),\end{aligned}\quad (4)$$

which is independent of θ (and can describe a stand-alone 2D system: See section VII). These equations may be solved exactly:

$$e \tan \phi = \tan \left(\frac{\dot{\gamma} t}{e + 1/e} + \kappa \right), \quad (5)$$

and

$$\tan \theta = \frac{C e}{\sqrt{e^2 \sin^2 \phi + \cos^2 \phi}}. \quad (6)$$

where C and κ are constants. The particle rotates in a non-uniform way about the z (vorticity) axis with period

$$T = \frac{2\pi}{\dot{\gamma}} \left(e + \frac{1}{e} \right) = \frac{4\pi}{\dot{\gamma} \sqrt{1 - \beta^2}}. \quad (7)$$

If shear is applied in the xz plane, $\mathbf{u} = \dot{\gamma} z \hat{\mathbf{x}}$, we get

$$\frac{d\theta}{dt} = \dot{\gamma} \left(\frac{1}{2}(1 - \beta) + \beta \cos^2 \theta \right) \cos \phi \quad (8)$$

$$\frac{d\phi}{dt} = -\frac{\dot{\gamma}}{2} (1 + \beta) \cot \theta \sin \phi. \quad (9)$$

Note that in this flow the equations for $\dot{\theta}$ and $\dot{\phi}$ are no longer decoupled. This configuration is, however, the best choice for solving the Fokker-Planck equation (see below).

III. LANGEVIN DESCRIPTION

To obtain the Langevin equations we take the equations for the Jeffery orbits given above and add rotational diffusion [19, 51–57]. As explained in Appendix A, one gets

$$\dot{\mathbf{p}} = (\mathbf{I} - \mathbf{p} \otimes \mathbf{p})(\beta \mathbf{E} + \mathbf{W})\mathbf{p} - 2D\mathbf{p} + \sqrt{2D}\mathbf{p} \times \boldsymbol{\xi}, \quad (10)$$

where $\boldsymbol{\xi}$ is a vectorial white noise and the additional term $-2D\mathbf{p}$ corresponds to the drift induced by the multiplicative noise (transformation from the Stratonovich to the Itô calculus). Note that this drift guarantees the conservation of the norm of the unit vector \mathbf{p} when Eq. (10) is interpreted in the Itô sense, as we assume in the following.

The Langevin equation can be expressed in Cartesian coordinates. In this case Eq. (10) corresponds to randomly displacing the point representing the orientation p in a plane tangent to the surface of the unit sphere and then scaling it back so that it again lies on the surface of the sphere.

However, in order to compare with the Fokker-Planck equation it is more convenient to express the Langevin equation directly in spherical polar coordinates. For pure diffusion the equations are the following [58, 59]:

$$\frac{d\theta}{dt} = \frac{D}{\tan \theta} + \sqrt{2D}\xi_1(t) \quad (11)$$

$$\frac{d\phi}{dt} = \frac{\sqrt{2D}}{\sin \theta} \xi_2(t), \quad (12)$$

where $\xi_1(t)$ and $\xi_2(t)$ are independent Gaussian white noises.

To perform numerical simulations of these equations we introduce a finite timestep δt to calculate the increments:

$$\theta(t + \delta t) = \theta(t) + \frac{D}{\tan \theta} \delta t + \sqrt{2D\delta t} \eta_1 \quad (13)$$

$$\phi(t + \delta t) = \phi(t) + \frac{\sqrt{2D\delta t}}{\sin \theta} \eta_2, \quad (14)$$

where $\eta_1(t)$ and $\eta_2(t)$ are normal variates with mean zero and standard deviation one ($\mathcal{N}(0, 1)$). We can check that this algorithm produces a uniform distribution of particle orientation over the surface of a sphere. While there are singularities at $\theta = 0, \pi$, their presence does not cause serious problems in the numerical simulations.

To simulate the Jeffery orbits with noise, we simply combine these equations with those for the Jeffery orbits (the Itô drift being unchanged). For shear in the xy plane we obtain

$$\theta(t + \delta t) = \theta(t) + \frac{\dot{\gamma}\beta}{4} \sin(2\theta) \sin(2\phi) \delta t + \frac{D}{\tan \theta} \delta t + \sqrt{2D\delta t} \eta_1 \quad (15)$$

$$\phi(t + \delta t) = \phi(t) - \frac{\dot{\gamma}}{2} (1 - \beta \cos(2\phi)) \delta t + \frac{\sqrt{2D\delta t}}{\sin \theta} \eta_2 \quad (16)$$

while for shear in the xz plane the result is

$$\theta(t + \delta t) = \theta(t) + \dot{\gamma} \left(\frac{1}{2}(1 - \beta) + \beta \cos^2 \theta \right) \cos \phi \delta t + \frac{D}{\tan \theta} \delta t + \sqrt{2D\delta t} \eta_1 \quad (17)$$

$$\phi(t + \delta t) = \phi(t) - \frac{\dot{\gamma}}{2} (1 + \beta) \cot \theta \sin \phi \delta t + \frac{\sqrt{2D\delta t}}{\sin \theta} \eta_2 \quad (18)$$

Of course changing the shear plane should not affect the results. For the same parameters β and Pe (or $D/\dot{\gamma} = 1/Pe$) we expect to obtain the same results in the two coordinate systems. Examples of Jeffery orbits with noise are given in Fig. 2.

IV. FOKKER-PLANCK DESCRIPTION

Let $\psi(\theta, \phi, t)$ be the probability density function of finding the particle with orientation (θ, ϕ) at time t . This satisfies the continuity equation

$$\hat{\Lambda} = -\frac{3}{2}\beta \sin(2\theta \cos \phi) + \left(\frac{1-\beta}{2} + \beta \cos^2 \theta \right) \cos \phi \frac{\partial}{\partial \theta} - \frac{1+\beta}{2} \cot \theta \sin \phi \frac{\partial}{\partial \phi} \quad (21)$$

Doi and Edwards studied a particular case, an infinitely thin needle, $\beta = 1$, for which

$$\hat{\Lambda}_1 = -3 \sin \theta \cos \theta \cos \phi + \cos^2 \theta \cos \phi \frac{\partial}{\partial \theta} - \cot \theta \sin \phi \frac{\partial}{\partial \phi} \quad (22)$$

or, in terms of the angular momentum operators:

$$\hat{\Lambda}_1 = \left[\sqrt{\frac{16\pi}{45}} Y_2^0 + \frac{1}{3} \right] i\hat{L}_y + \sqrt{\frac{2\pi}{15}} (Y_2^1 + Y_2^{-1}) \hat{L}_z + 3\sqrt{\frac{2\pi}{15}} (Y_2^1 - Y_2^{-1}) \quad (23)$$

where $\hat{L}_y = i(-\cos \phi \partial/\partial \theta + \cot \theta \sin \phi \partial/\partial \phi)$ and $\hat{L}_z = -i\partial/\partial \phi$. Here we extend the Doi and Edwards solution to arbitrary values of β by noting that the operator can be expressed as

$$\hat{\Lambda} = \beta \hat{\Lambda}_1 + \frac{1-\beta}{2} i\hat{L}_y \quad (24)$$

For $\beta = 0$, corresponding to a sphere, Eq. (20) simplifies to

$$i\hat{L}_y \psi(\theta, \phi) = 2\epsilon \nabla^2 \psi(\theta, \phi) \quad (25)$$

whose solution is $\psi(\theta, \phi) = 1/4\pi$. To solve the FP equation for any value of β , following Doi and Edwards, we introduce the functions

$$S_l^m(\theta, \phi) = \frac{1}{\sqrt{2}} [Y_l^m(\theta, \phi) + (-1)^m Y_l^{-m}(\theta, \phi)], \quad (26)$$

also known as real spherical harmonics, which are real and have the property that $S_l^m(\theta, -\phi) = S_l^m(\theta, \phi)$. The basis set is defined as

$$\frac{\partial \psi}{\partial t} = -\nabla \cdot (\mathbf{w}\psi) + \nabla \cdot (D\nabla\psi) \quad (19)$$

where $\mathbf{w}(\theta, \phi) = (0, \dot{\theta}, \dot{\phi} \sin \theta)$, D is the rotational diffusion coefficient, assumed constant [41, 43].

It is convenient to solve the Fokker-Planck equation with shear ($\mathbf{v}\text{-grad } \mathbf{v}$) in the xz plane, which exploits the higher symmetry of the system with spherical coordinates (the reflection symmetry in the xz plane allows one to use real spherical harmonics). We obtain

$$\hat{\Lambda}\psi(\theta, \phi) = \epsilon \nabla^2 \psi \quad (20)$$

where $\epsilon = D/\dot{\gamma}$ and

$$|lm\rangle = \begin{cases} Y_l^m(\theta, \phi), & m = 0 \\ S_l^m(\theta, \phi), & m \neq 0 \end{cases} \quad (27)$$

with the property

$$\langle l'm' | lm \rangle = \delta_{l'l'} \delta_{m'm'} \quad (28)$$

We write the distribution function as

$$\psi(\theta, \phi) = \sum_{l \text{ even}}^{\infty} \sum_{m=0}^l b_{lm} |lm\rangle \quad (29)$$

This expansion has the required properties that $\psi(\pi - \theta, \phi + \pi) = \psi(\theta, \phi)$ (even parity) and $\psi(\theta, -\phi) = \psi(\theta, \phi)$ (reflection symmetry in the xz plane).

Substituting Eqs. (29) and (24) in Eq. (20) we obtain

$$Dl(l+1)b_{lm} = - \sum_{l' \geq 0, \text{ even}}^{l_{max}} \sum_{m'=0}^{l'} (lm | \hat{\Lambda} | l'm') b_{l'm'} \quad (30)$$

From this we generate $l_{max}(1 + l_{max}/4)$ simultaneous equations that can be solved to find the coefficients $\{b_{lm}\}$.

For convenience the expression of $\langle lm | \hat{\Lambda} | l'm' \rangle$ matrix elements are given in Appendix B. With these results the eigenfunction expansion of the exact distribution for particles with arbitrary shape factor can easily be obtained for any (reasonable) value of l_{max} without the need to evaluate the matrix elements by numerical integration.

V. PROPERTIES OF INTEREST

A. Trajectories

Figure 2 illustrates the effect of Brownian motion on Jeffery orbits for particles of shape parameters $\beta = 0.5, 0.8, 0.95$ (corresponding to elongations of $e = 1.73, 3, 6.24$). The trajectories were calculated from Langevin simulations using a timestep of 0.001 starting from an orientation of $\phi = \theta = \pi/3$. For zero noise, one recovers the unperturbed Jeffery orbits with their characteristic kayaking motion. For very small noise, $D/\dot{\gamma} = 0.0001$, one observes a small drift from the initial orbit, but the general shape remains similar to the unperturbed case. For a ten-fold increase in noise, one starts to see a concentration of the trajectories along the flow direction (x) and this effect becomes more pronounced as the particle elongation increases. With a still larger noise of $D/\dot{\gamma} = 0.01$ the fractal nature of the trajectories is apparent as they become increasingly aligned with the flow direction with only occasional excursions to the antipodean orientation.

B. Rotation around the vorticity axis

We first examine the rotation of the particle around the vorticity axis. For shear in the xy plane, in the steady state we have $\langle d\theta/dt \rangle = 0$ and

$$\frac{\dot{\gamma}\beta}{4} \langle \sin(2\theta) \sin(2\phi) \rangle + D \langle \cot \theta \rangle = 0 \quad (31)$$

and

$$\left\langle \frac{d\phi}{dt} \right\rangle = -\frac{\dot{\gamma}}{2} (1 - \beta \langle \cos(2\phi) \rangle) \quad (32)$$

With zero noise we find using Eq. (5)

$$\left\langle \frac{d\phi}{dt} \right\rangle = -\frac{\dot{\gamma}e}{e^2 + 1} = -\frac{\dot{\gamma}}{2} \sqrt{1 - \beta^2} \quad (33)$$

Interestingly this implies that the infinitely thin particles, $\beta = 1$, do not rotate at all, while a spherical particle, $\beta = 0$, rotates at $\dot{\gamma}/2$. Fig. 3 shows some simulation results and, for all values of β , the rate of rotation decreases with increasing noise. Perturbation theory, as developed in Appendix C, can be used to calculate the rotation speed in the limit of large noise (or small Pe).

C. Orientational distribution function

We present probability density functions of the particle orientation obtained from Langevin simulations as heat maps in Figs. 4 and 5. Figure 4 is for a needle, $\beta = 1$, with $Pe = 100$ for three perpendicular v -grad v planes, xy , xz and yz . At this relatively high Péclet num-

ber the orientational distribution is strongly anisotropic. For the case with shear in the xy plane the peak of the distribution is centered in the same plane. It does not point directly along the x axis, but is rotated towards the y -axis. The spot is not symmetric, being somewhat stretched in the z direction. It is clear that the remaining distributions xz and yz are related to the first one by a simple rotation. This helps to confirm the correct functioning of the Langevin algorithm as well as the graphical representation.

In Fig. 5 (left) we show the effect of varying the Péclet number between 1 and 100 for particles with shape parameters $\beta = 0.5, 0.8$ and 1. As expected, with increasing noise (decreasing Pe) the distributions spread. For a fixed value of Pe the distribution becomes more diffuse as the particle becomes less elongated.

These numerical solutions can be compared with the solutions of the Fokker-Planck equation. Fig. 5 (right) shows the probability surfaces for the solution of the Fokker-Planck equation (29) with $l_{max} = 10$ for the same Péclet numbers. The solution was obtained with shear in the xz plane.

D. Order Matrix

The orientational order can be characterized with the order matrix [60]

$$\mathbf{Q} = \int_{S^2} \left(\mathbf{p} \otimes \mathbf{p} - \frac{\mathbf{I}}{3} \right) \psi(\mathbf{p}) d\mathbf{p} \quad (34)$$

where \mathbf{I} is the unit matrix and $\mathbf{p} = (\sin \theta \cos \phi, \sin \theta \sin \phi, \cos \theta)$. It follows from the definition that \mathbf{Q} is a symmetric, traceless 3×3 matrix. It can be expressed in terms of a triad of orthonormal vectors

$$\mathbf{Q} = \lambda_1 \mathbf{e}_1 \otimes \mathbf{e}_1 + \lambda_2 \mathbf{e}_2 \otimes \mathbf{e}_2 + \lambda_3 \mathbf{e}_3 \otimes \mathbf{e}_3 \quad (35)$$

with $\lambda_1 + \lambda_2 + \lambda_3 = 0$. Three kinds of order are possible: (i) isotropic with all eigenvalues equal to zero; (ii) uniaxial with one positive eigenvalue and two equal negative eigenvalues (or two equal positive and one negative, where the preferred orientation is along a plane instead of along a direction. We observe the latter near flat walls for rod-like particles) and (iii) biaxial with three distinct eigenvalues. The eigenvalues satisfy $-1/3 \leq \lambda_i \leq 2/3$.

The \mathbf{Q} -matrix may be represented as

$$\mathbf{Q} = s \left(\mathbf{e}_1 \otimes \mathbf{e}_1 - \frac{\mathbf{I}}{3} \right) + r \left(\mathbf{e}_2 \otimes \mathbf{e}_2 - \frac{\mathbf{I}}{3} \right) \quad (36)$$

with the scalar order parameters (s, r) describing nematic ordering and biaxiality, given by

$$s = 2\lambda_1 + \lambda_2, \quad r = 2\lambda_2 + \lambda_1, \quad (37)$$

assuming that the eigenvalues are labeled so that $\lambda_1 \geq \lambda_2 \geq \lambda_3$. (An alternative representation of the \mathbf{Q} tensor

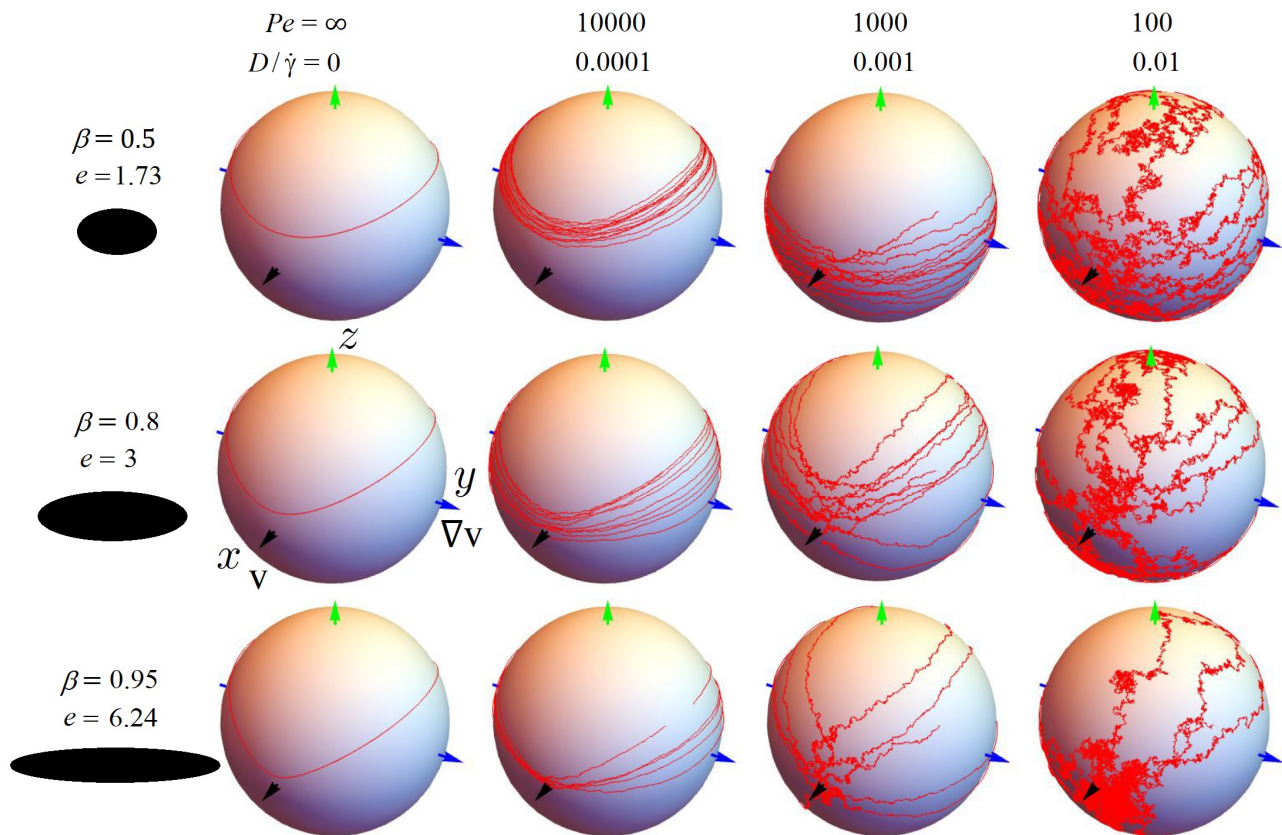


FIG. 2: Trajectory plots with shear v - $\text{grad } v$ in the xy plane from numerical simulation for different elongations. In all cases the starting orientation is $\theta = \phi = \pi/3$.

[61] gives rise to another set of parameters, $S = 3\lambda_1/2$, the widely used uniaxial nematic order parameter, and $T = (2\lambda_2 + \lambda_1)/2$, an alternative measure of biaxiality. The two sets are related by $S = s - r/2, T = r/2$. For a uniaxial system there is no difference, $s = S$.

In the simulations the order tensor is evaluated by computing the tensor product $\mathbf{p} \otimes \mathbf{p}$ averaged over the time steps. We can calculate it from the Fokker-Planck equation by substituting the orientational probability function, Eq. (29), in Eq. (34) to obtain

$$\mathbf{Q} = \begin{pmatrix} \sqrt{\frac{4\pi}{45}}(\sqrt{3}b_{22} - b_{20}) & 0 & -\sqrt{\frac{4\pi}{15}}b_{21} \\ 0 & -\sqrt{\frac{4\pi}{45}}(\sqrt{3}b_{22} + b_{20}) & 0 \\ -\sqrt{\frac{4\pi}{15}}b_{21} & 0 & 2\sqrt{\frac{4\pi}{45}}b_{20} \end{pmatrix}, \quad (38)$$

indicating that the order matrix depends only on the second moments of the distribution b_{20}, b_{21}, b_{22} . To obtain these one chooses a value of l_{\max} and then constructs the $l_{\max}(1 + l_{\max}/4)/2$ simultaneous equations (30) that are solved for b_{lm} . The values of b_{20}, b_{21}, b_{22} depend on Pe and l_{\max} : see Fig. 6. We typically used $l_{\max} = 24 - 36$ in the results presented here.

We also use perturbation theory to obtain analytical expressions for s and r valid at low noise. This involves expanding the orientational distribution function as a

power series in either β or Pe . With the former we obtain $s = 2r = \frac{2\beta}{5\sqrt{1+36(D/\dot{\gamma})^2}}$ while the latter yields $s = 2r = \beta Pe/15$. Details of the calculations are presented in Appendices C and D.

Figure 7 shows the scalar order parameters s and r for $\beta = 1, 0.95, 0.9$ calculated from the simulations, the series solution of the FP equation (using $l_{\max} = 24$) and β -perturbation theory for $0.01 \leq D/\dot{\gamma} \leq 1$. The simulations were performed for 5×10^6 steps with a timestep of

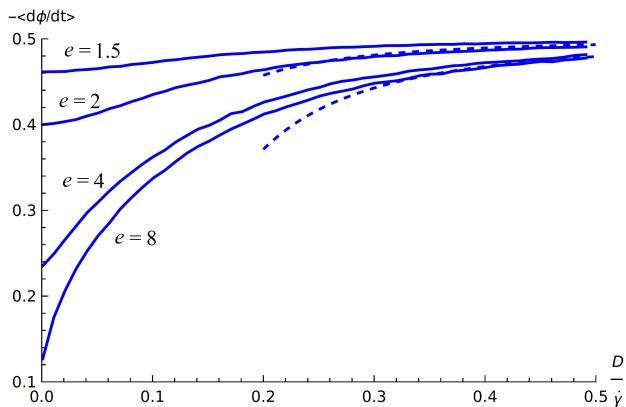


FIG. 3: Mean angular velocity for particle elongations $e = 1.5, 2, 4, 8$, calculated from simulations with shear in the xy plane. The limiting values for small D are correctly given by Eq. (33). The dashed lines show the results of perturbation theory to second order (Appendix C).

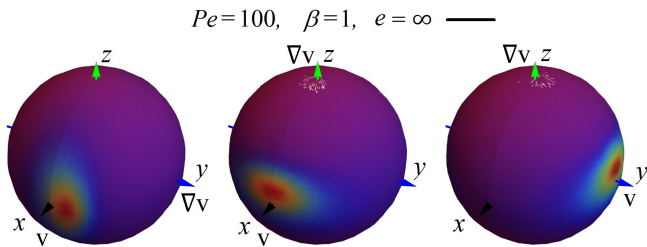


FIG. 4: Density plots of the particle orientation from Langevin simulations with v -grad v in the xy , xz and yz planes for $Pe = 100$ and $\beta = 1$.

$\delta t = 0.001$. We verified that the simulation results do not depend on the choice of the shear plane. For both s and r the simulation results are in agreement with the FP equation for a wide range of $D/\dot{\gamma}$. The value of r (biaxiality) computed from the simulations displays larger fluctuations than the value of s . Interestingly, both the solution of the FP equation and simulation exhibit a maximum value of r for $D/\dot{\gamma} \approx 0.05$ for $\beta > 0.9$. Perturbation theory provides an excellent description of the nematic ordering s for $D/\dot{\gamma} > 0.1$. It does not work as well as for describing the biaxiality (r does not exhibit a maximum), but does approach the simulation results as $D/\dot{\gamma}$ increases.

The overall decreasing trend of s with $D/\dot{\gamma}$ is what we would expect: noise generally reduces nematic ordering, leading to smaller values of s . Regarding the biaxiality the situation is more complex: for large noise r is expected to decrease with noise as in the large noise limit the system is expected to become isotropic. In the limit of small noise however, where the value of s is increasing and for very elongated particles it converges to 1 the

value of r should converge to 0 by definition. This is what we see in the small noise limit in Figs. 7(b,d).

We analyzed the behavior of the nematic ordering and the biaxiality for Jeffery orbits without noise using the procedure outlined in Appendix E. The results are shown in Fig. 8. While the value of s increases more and more rapidly as β approaches one, r displays a maximum at $\beta = 0.876$ before rapidly decreasing to zero.

VI. IN- AND OUT-OF PLANE DISTRIBUTIONS

In addition to the full orientational distributions described above, it is useful to examine the angular distribution of the particle in the v -grad v plane as well as in the perpendicular (vorticity) direction. This can be done most easily using the simulation algorithm with the shear in the (x, y) plane. In this case the orientation of the particle in the v -grad v plane is specified by ϕ and the orientation in the perpendicular plane is given by $\delta = \pi/2 - \theta$. The corresponding distributions, denoted by $f_{\parallel}(\phi)$ and $f_{\perp}(\delta)$ respectively, are the marginal distributions of the full orientational distribution:

$$f_{\parallel}(\phi) = \int_0^{\pi} \psi(\theta, \phi) \sin \theta d\theta; \quad f_{\perp}(\delta) = \int_0^{2\pi} \psi(\delta, \phi) d\phi \quad (39)$$

Results for three different Bretherton parameters, $\beta = 0.5, 0.8, 1$ (corresponding to elongations $e = \sqrt{3}, 3, \infty$), each for $Pe = 1, 10, 50, 100$, are shown in Fig. 9.

For large noise ($Pe = 1$), the out of plane distribution $f_{\perp}(\delta)$ is basically equal to the uniform distribution ($\cos \delta$) for all three particle shapes. The in-plane distribution $f_{\parallel}(\phi)$ is not perfectly uniform. Rather, it has a slight modulation, which has similar amplitude for the three types of grains. The peak of the distribution is located at around 45 degrees, which is in accordance with 2D calculations by Marschall et al. [13] and other data [62].

For the least elongated particle ($\beta = 0.5$) decreasing the amplitude of the noise results in only a minor change in $f_{\perp}(\delta)$, while $f_{\parallel}(\phi)$ changes significantly. Decreasing noise leads to a sharper maximum and a shift of the maximum towards 0. The out-of-plane distribution is very similar to a uniform distribution, irrespective of the amplitude of the noise. This means that decreasing noise does not drive the particles into the v -grad v plane.

For a longer particle ($e = 3$) both distributions $f_{\perp}(\delta)$ and $f_{\parallel}(\phi)$ change with decreasing amplitude of the noise. The in-plane distribution $f_{\parallel}(\phi)$ becomes notably sharper than for $e = 1.73$. The average angle appears to be larger for $e = 3$ than for $e = 1.73$, as observed by Marschall et al. [13]. The peak of $f_{\perp}(\delta)$ also becomes larger, meaning that for smaller noise the $e = 3$ particles have a greater tendency to remain in the proximity of the v -grad v plane than the $e = 1.73$ particles.

For very long particles ($e = \infty; \beta = 1$) decreasing noise results in sharper peaks for both the in-plane and

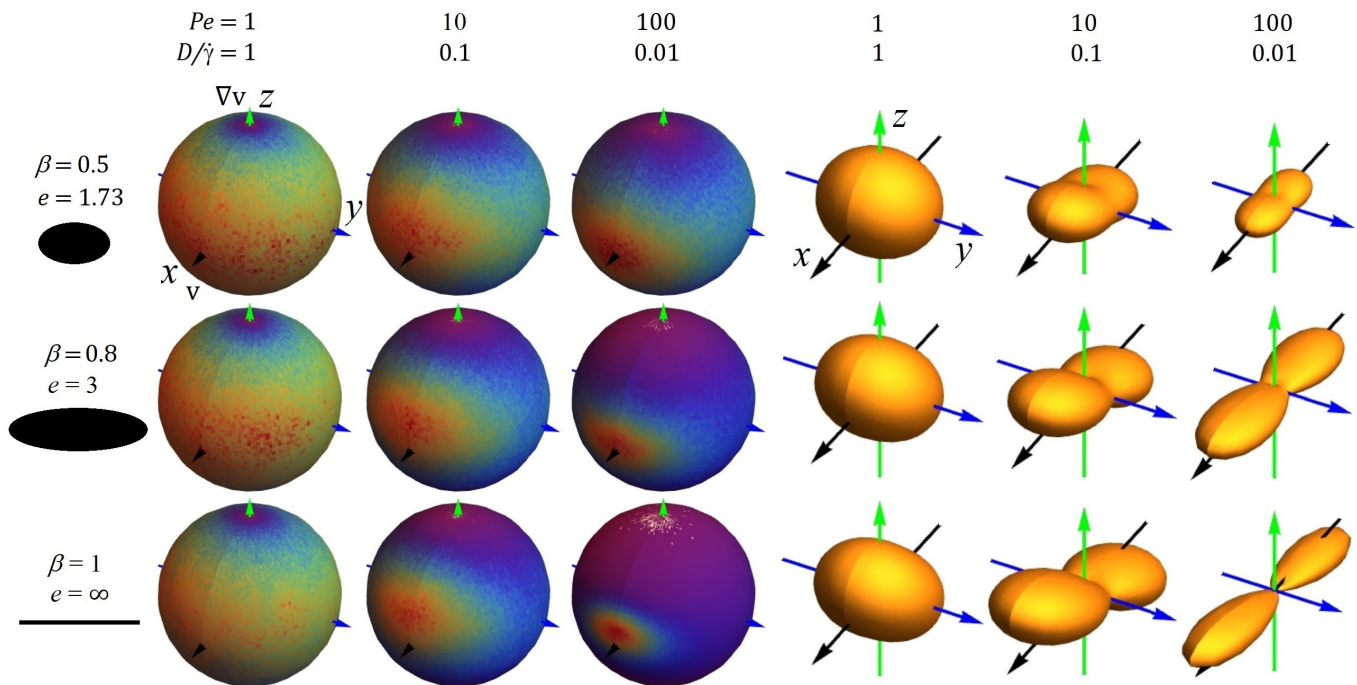


FIG. 5: Left: Density plots of the particle orientation calculated from Langevin simulations with v -grad v in the xz plane, right: Probability surface of the particle orientation calculated from the solution of the Fokker-Planck equation, Eq. (29) with $l_{max} = 10$. For the probability surfaces the distance of the surface from the origin in a given direction is proportional to the probability of the particle orientation in that direction.

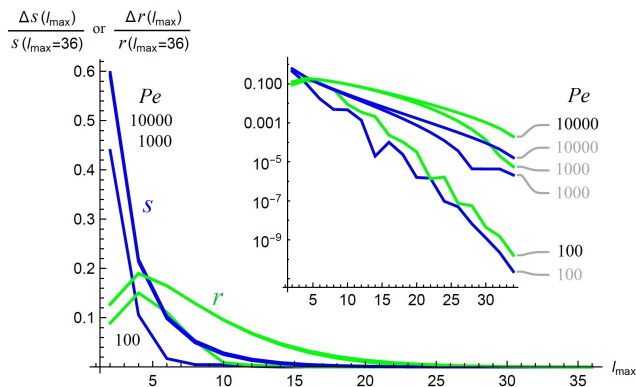


FIG. 6: Convergence of the scalar order parameters s (blue) and r (green) as a function of l_{max} for $Pe = 100, 1000, 10000$, curves from bottom to top, respectively.

out-of-plane orientation distributions. This means that decreasing noise not only leads to strong ordering in the v -grad v plane, but the particles are also clearly driven towards the the v -grad v plane.

The circular mean of the in-plane orientation, $\langle \phi \rangle_{CM}$, is shown as a function of $D/\dot{\gamma} = 1/Pe$ in Fig. 10(a). The behavior is similar to the result obtained by Marschall et

al. [13] for a strictly two-dimensional system, that is the mean angle increases with noise ($D/\dot{\gamma}$) and tends to an asymptotic value of $\pi/4$. For a given value of $D/\dot{\gamma}$ the mean angle increases with increasing particle elongation.

For the out-of-plane distribution the mean angle is always zero (no symmetry breaking). We show the (standard) variance, $\langle \delta^2 \rangle$ as a function of $D/\dot{\gamma} = 1/Pe$ in Fig. 10(b). All the curves tend to the value corresponding to a uniform distribution $(\pi^2 - 8)/4$ as the noise increases. For the particle of elongation $e = 1.5$ the distribution is nearly uniform for all values of the noise and, consequently, the variance shows little variation. For $e = 2$ the variance is a non-monotonic function of $D/\dot{\gamma}$, with a minimum value at about $D/\dot{\gamma} = 0.5$. More elongated particles display a strongly peaked distribution, yielding a small variance, for small values of $D/\dot{\gamma}$.

VII. TWO DIMENSIONS

For completeness we now present results for the purely two-dimensional motion of an anisometric particle in a shear flow. This case has recently been studied by Marschall et al. [13] using numerical solutions of the Langevin equation. Here we present the solution of the corresponding Fokker-Planck equation.

The overdamped Langevin equation for the orientation

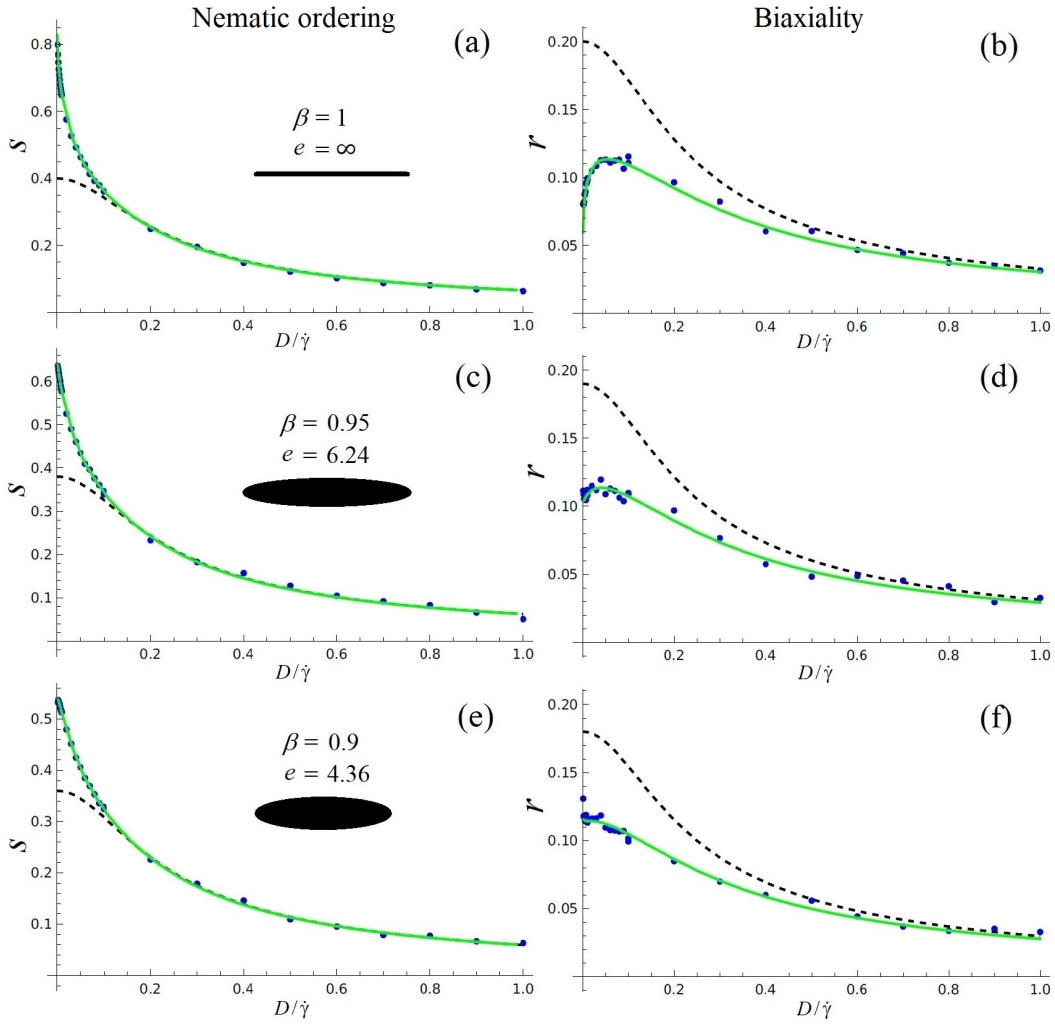


FIG. 7: Scalar order parameters s and r as a function of $D/\dot{\gamma}$. FP equation (green); β perturbation theory (dashed); Langevin simulations xz (blue).

of the particle at time t can be written as

$$\frac{d\phi}{dt} = f(\phi) + \sqrt{2D}\xi, \quad (40)$$

where ξ is Gaussian white noise and

$$f(\phi) = -\frac{1}{2}\dot{\gamma}(1 - \beta \cos 2\phi), \quad (41)$$

where β has the same definition as in 3D. Moreover, due to the decoupling of ϕ and θ in 3D for v -grad v in the xy plane, the form of $f(\phi)$ is the same as in Eq. (4). Note that with this choice, the major axis of the ellipse is parallel to the flow when $\phi = 0$. The sign of the function $f(\phi)$ is chosen so that the particle rotates in the clockwise sense.

The corresponding Fokker-Planck equation for the orientational distribution, $\psi(\theta, t)$, is

$$\frac{\partial \psi(\theta, t)}{\partial t} = -\frac{\partial}{\partial \phi} [f(\phi)\psi(\phi, t)] + \epsilon \frac{\partial^2 \psi(\phi, t)}{\partial \phi^2}. \quad (42)$$

Let us first focus on the steady state for which

$$\frac{d}{d\phi} [f(\phi)\psi(\phi)] = \epsilon \frac{d^2 \psi}{d\phi^2}. \quad (43)$$

Integrating once we obtain

$$f(\phi)\psi(\phi) = \epsilon \frac{d\psi}{d\phi} + c \quad (44)$$

If there is no noise $D/\dot{\gamma} = 0$ and

$$f(\phi)\psi(\phi) = c. \quad (45)$$

This simple equation expresses the fact that the probability to find the particle at a given angle is inversely proportional to its instantaneous angular velocity.

From the normalization condition

$$\int_{-\pi/2}^{\pi/2} d\phi \psi(\phi) = 1 \quad (46)$$

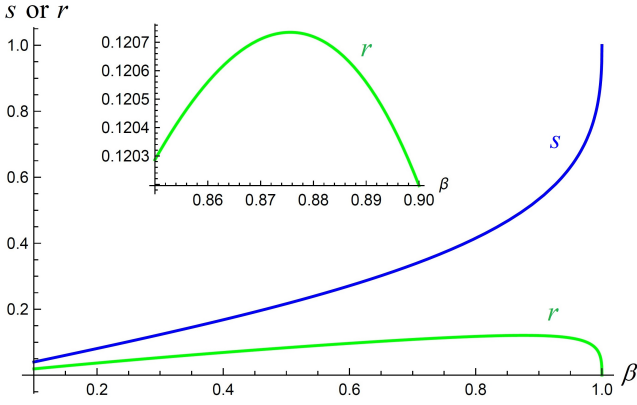


FIG. 8: Scalar order parameters s (blue) and r (green) of Jeffery orbits without noise averaged over the initial orientation as a function of β .

we find that $c = \dot{\gamma} \frac{\epsilon}{\pi(e^2+1)}$, so

$$\psi_0(\phi) = \frac{e}{\pi(1 + (e^2 - 1) \sin^2 \phi)}. \quad (47)$$

This is a symmetric function, $\psi_0(-\phi) = \psi_0(\phi)$ with a maximum value of e/π at $\phi = 0$ and a minimum value of $1/(e\pi)$ at $\phi = \pm\pi/2$. It is also independent of the shear rate.

Various approaches can be used to solve Eq. (42) including expansion in circular harmonics, a direct method and singular perturbation theory. We focus on the first as it corresponds to method used in 3D. The direct solution only works in 2D where it gives the same results as the circular expansion method. Perturbation theory is more limited, but it can give information in the limit of small noise.

A. Solution using circular harmonic expansion

Since $\psi(\phi)$ is a periodic function on the interval $-\pi/2 < \phi < \pi/2$ it may be expanded in circular harmonics:

$$\psi(\phi) = \sum_{k=0} a_k \cos(2k\phi) + b_k \sin(2k\phi), \quad (48)$$

that clearly satisfies $\psi(-\pi/2) = \psi(\pi/2)$. The normalization condition requires that $a_0 = 1/\pi$. Also $b_0 = 0$. Given the distribution function the coefficients can be obtained as

$$\begin{aligned} a_k &= \frac{2}{\pi} \int_{-\pi/2}^{\pi/2} \cos(2k\theta) \psi(\theta) d\theta \\ b_k &= \frac{2}{\pi} \int_{-\pi/2}^{\pi/2} \sin(2k\theta) \psi(\theta) d\theta. \end{aligned} \quad (49)$$

Let us first apply this to the known solution in the absence of noise, $\psi_0(\theta)$. Since this function is symmetric

$b_k = 0$ for all k . The coefficients of the cosine terms are obtained from

$$a_m = \frac{2}{\pi} \left(\frac{e-1}{e+1} \right)^m, \quad m \geq 1. \quad (50)$$

Now to obtain the solution in the presence of noise we write the FP equation in the form

$$\frac{d}{d\phi} [(1 - \beta \cos 2\phi) \psi(\phi)] = -2\epsilon \frac{d^2 \psi}{d\phi^2}, \quad (51)$$

where we have used the relation $\sin^2 \phi = \frac{1}{2}(1 - \cos 2\phi)$. Substituting Eq. (48) in Eq. (51), expressing the result entirely in terms of the basis functions $\cos 2k\phi$ and $\sin 2k\phi$ and equating their coefficients we find

$$2b_k - \beta(b_{k-1} + b_{k+1}) = 8\epsilon k a_k \quad (52)$$

and

$$-2a_k + \beta((1 + \delta_{k,1})a_{k-1} + a_{k+1}) = 8\epsilon k b_k \quad (53)$$

for the cosine and sine terms respectively, where $\delta_{k,1}$ is the Kronecker delta. We obtain a numerical solution by taking the first n terms in the expansion, Eq. (48), giving $2n$ equations. We then set $a_{n+1} = 0$ and $b_{n+1} = 0$ in the last two equations with $k = n$. We have a linear system that can be solved in the unknowns a_i, b_i , $i = 1, n$. Convergence of the series is rapid, but more terms are required as the elongation increases. With $e = 8$ in the noiseless case, for $n = 8$ spurious oscillations are present, but for $n = 24$ the series solution is indistinguishable from the exact solution, Eq. (47). Some examples of the distribution are shown in Fig. 11.

B. Perturbation Theory

We can apply singular perturbation theory to the Fokker-Planck equation (43) to obtain the behavior at small noise. Taking $\epsilon = D/\dot{\gamma}$ as a small parameter:

$$\psi(\phi, \epsilon) = \psi_0(\phi) + \epsilon \psi_1(\phi) + \epsilon^2 \psi_2(\phi) + \dots, \quad (54)$$

where $\psi_0(\phi)$ is the solution to the unperturbed problem. Substituting in Eq. (51) we obtain

$$f(\phi)(\psi_0 + \epsilon \psi_1 + \dots) = \epsilon \frac{d\psi_0}{d\phi} + \epsilon^2 \frac{d\psi_1}{d\phi} + \dots + c. \quad (55)$$

Equating terms with the same power of ϵ we obtain

$$f(\phi)\psi_0(\phi) = c, \quad f(\phi)\psi_1(\phi) = \frac{d\psi_0}{d\phi}, \quad f(\phi)\psi_2(\phi) = \frac{d\psi_1}{d\phi}, \dots \quad (56)$$

Explicitly, at first order we find

$$\psi_1(\phi) = -\frac{e(e^4 - 1) \sin 2\phi}{\pi((e^2 - 1) \sin^2 \phi + 1)^3}. \quad (57)$$

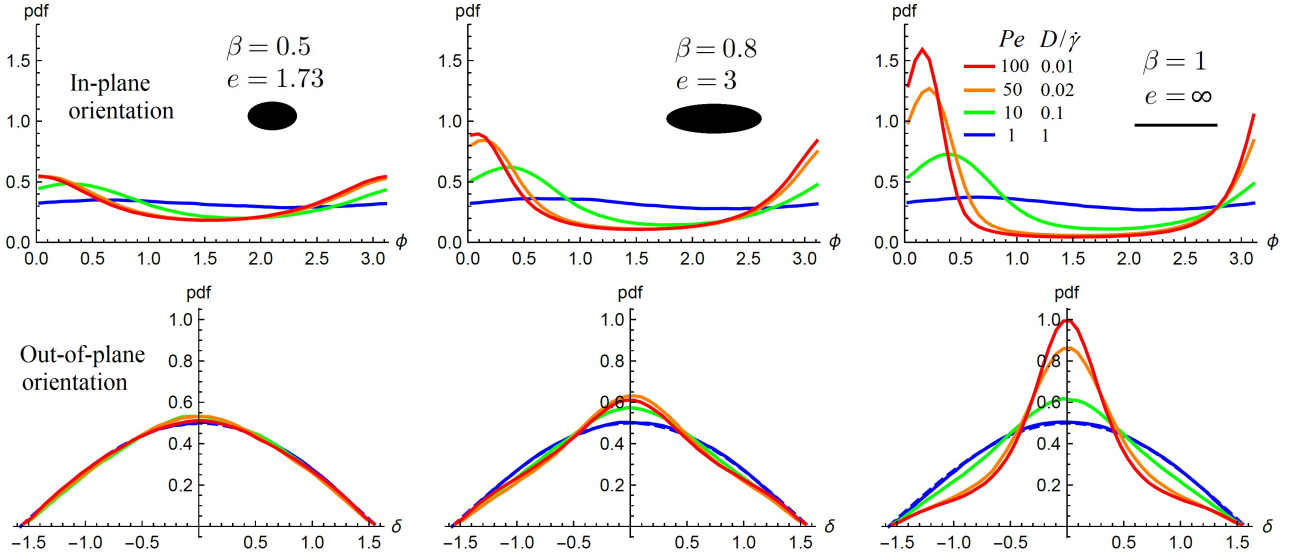


FIG. 9: In-plane (upper row) and out-of-plane (bottom row) orientational distributions for $Pe = 1, 10, 50, 100$, for three different particle elongations, calculated from Langevin simulations with shear in the xy plane. The dashed curve shows the out-of-plane distribution ($\cos \delta$) for a system with random orientation

We note that $\int_{-\pi/2}^{\pi/2} d\phi \psi_0(\phi) = 1$ and $\int_{-\pi/2}^{\pi/2} d\phi \psi_1(\phi) = 0$, but $\int_{-\pi/2}^{\pi/2} d\phi \psi_2(\phi) \neq 0$. Thus perturbation theory to first order in ϵ , $\psi(\phi, \epsilon) = \psi_0(\phi) + \epsilon\psi_1(\phi)$, gives directly a normalized distribution. Adding the second order term, $\psi_2(\phi)$ results in a non-normalized distribution. One could, of course, renormalize this result. Also note that, even for a modest elongation of $e = 1.5$ the amplitude of $\psi_k(\phi)$ increases rapidly with k . So we expect to obtain good results only for small ϵ .

Similarly, we can also use perturbation theory to obtain the behavior at large noise by taking Pe as the expansion parameter:

$$\psi(\phi, Pe) = \psi_0 + Pe\psi_1(\phi) + Pe^2\psi_2(\phi) + \dots \quad (58)$$

where $\psi_0 = 1/\pi$ is the (uniform) distribution in the limit of large noise. Following the same procedure as above we obtain

$$\psi_1(\phi) = \frac{\beta}{4\pi} \sin(2\phi) \quad (59)$$

$$\psi_2(\phi) = \frac{\beta}{32\pi} \cos(2\phi)(2 - \beta \cos(2\phi)). \quad (60)$$

From these results we calculate

$$\langle \cos(2\phi) \rangle = \frac{\beta}{32} Pe^2 + O(Pe^3). \quad (61)$$

The corresponding results for the 3D system are presented in Appendices C and D.

C. Mean angular velocity

To find the mean angular velocity we take the average of Eq. (40)

$$\left\langle \frac{d\phi}{dt} \right\rangle = -\frac{\dot{\gamma}}{2} (1 - \beta \langle \cos 2\phi \rangle) = -\frac{\dot{\gamma}}{2} \left(1 - \frac{\pi}{2} \beta a_1\right). \quad (62)$$

For $\epsilon = 0$, $a_1 = \frac{2}{\pi} \frac{e-1}{e+1}$ giving

$$\left\langle \frac{d\phi}{dt} \right\rangle_{\epsilon=0} = -\dot{\gamma} \frac{e}{e^2 + 1}, \quad (63)$$

which is the same as the 3D system, Eq. (33). In the limit of large noise we find

$$\left\langle \frac{d\phi}{dt} \right\rangle_{\epsilon=\infty} = -\frac{\dot{\gamma}}{2}. \quad (64)$$

The numerical results shown in Fig. 12(a) vary smoothly between these two limits. We also confirm that a perturbation theory estimate, obtained by substituting Eq. (61) in Eq. (62), describes the behavior at large noise.

It is instructive to compare the two-dimensional system with the three-dimensional one, Fig. 12(b). The limiting behavior for small and large values of $D/\dot{\gamma}$ is the same, but for intermediate values, the mean angular velocity is higher in 3D.

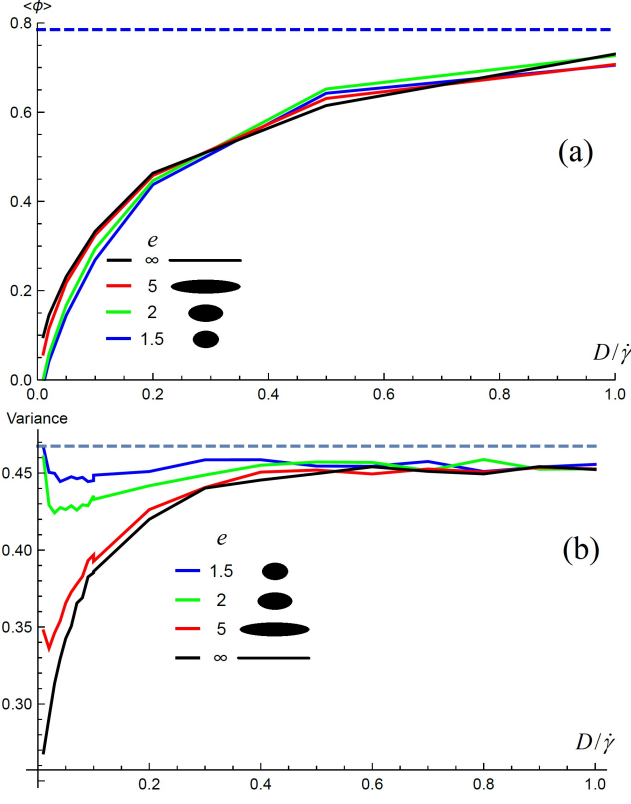


FIG. 10: (a) Circular mean of the in-plane orientation for $e = 1.5, 2, 5, \infty$ ($\beta = 1$). The dashed line is $\pi/4$; (b) Variance of out-of-plane orientation for $e = 1.5, 2, 5, \infty$ ($\beta = 1$). The dashed line is the value for a random distribution, $(\pi^2 - 8)/4$.

D. Orientational Order Matrix

To quantify the ordering we can evaluate the orientational order matrix

$$Q = \begin{bmatrix} \langle \cos 2\theta \rangle & \langle \sin 2\theta \rangle \\ \langle \sin 2\theta \rangle & -\langle \cos 2\theta \rangle \end{bmatrix} \quad (65)$$

The matrix has two eigenvalues, $\pm S$, where S is the nematic order parameter, and the corresponding eigenvectors are

$$\begin{pmatrix} \cos \theta_p \\ \sin \theta_p \end{pmatrix} \text{ and } \begin{pmatrix} -\sin \theta_p \\ \cos \theta_p \end{pmatrix} \quad (66)$$

Due to asymmetry, the maximum of the distribution does not necessarily occur at $\theta = \theta_p$. The angle at which the distribution displays a maximum, θ_{\max} , and the eigenvector orientation, θ_p , are equal in the limits of large and small noise. At intermediate noise, $\theta_p < \theta_{\max}$.

When $\psi(\theta)$ is expressed using the circular harmonic expansion, Eq. (48), the ordering matrix is

$$Q = \frac{\pi}{2} \begin{bmatrix} a_1 & b_1 \\ b_1 & -a_1 \end{bmatrix} \quad (67)$$

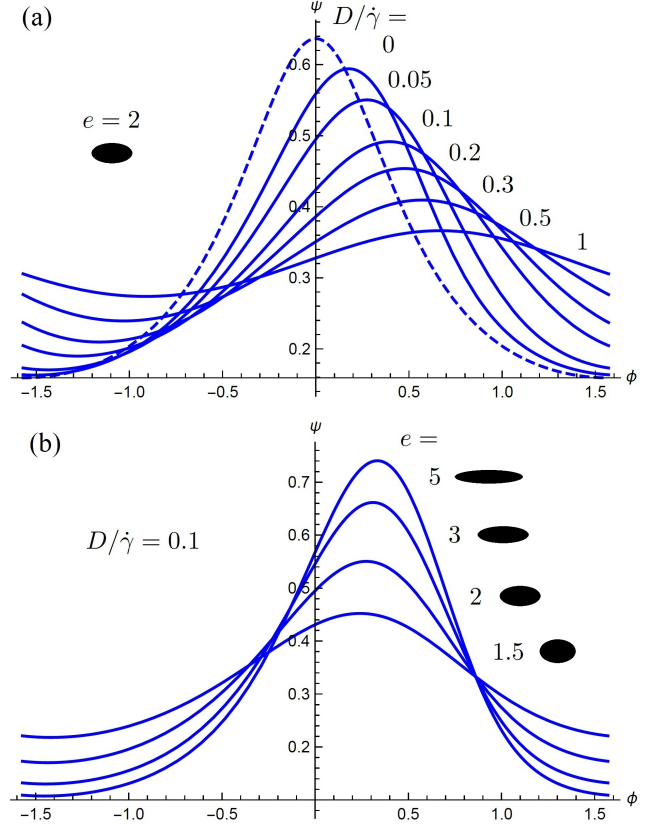


FIG. 11: Orientational distributions in 2D. (a) $e = 2$ and $D/\dot{\gamma} = 0.05, 0.1, 0.2, 0.3, 0.5, 1$. The dashed line shows the distribution without noise. (b) $D/\dot{\gamma} = 0.1$ and $e = 1.5, 2, 3, 5$.

Applying perturbation theory to second order results in

$$S = \frac{e-1}{e+1} - c(e)\epsilon^2 + O(\epsilon^3) \quad (68)$$

with $c(e) = (1 + e^2)^2(5e^8 + 2e^6 - 8e^5 + 8e^3 - 2e^2 - 5)/32e^6$. This, however, provides a good description only for weakly elongated particles at small values of ϵ , see Fig. 13.

The orientation of the director, θ_p , can be computed from

$$\tan 2\theta_p = \frac{\langle \sin 2\theta \rangle}{\langle \cos 2\theta \rangle} = \frac{b_1}{a_1} \quad (69)$$

To obtain the Taylor series expansion to order ϵ we proceed as above with the result:

$$\tan 2\theta_p = \frac{(1+e)^2(1+e^2)}{2e^2} \epsilon + O(\epsilon^2) \quad (70)$$

Fig. 14 shows that θ_p increases monotonically with $\epsilon = D/\dot{\gamma}$ and approaches an asymptotic value of $\pi/4$ in the limit of large noise. While θ_p shows some variation with elongation at low noise levels, it is insensitive to elongation at higher levels of noise.

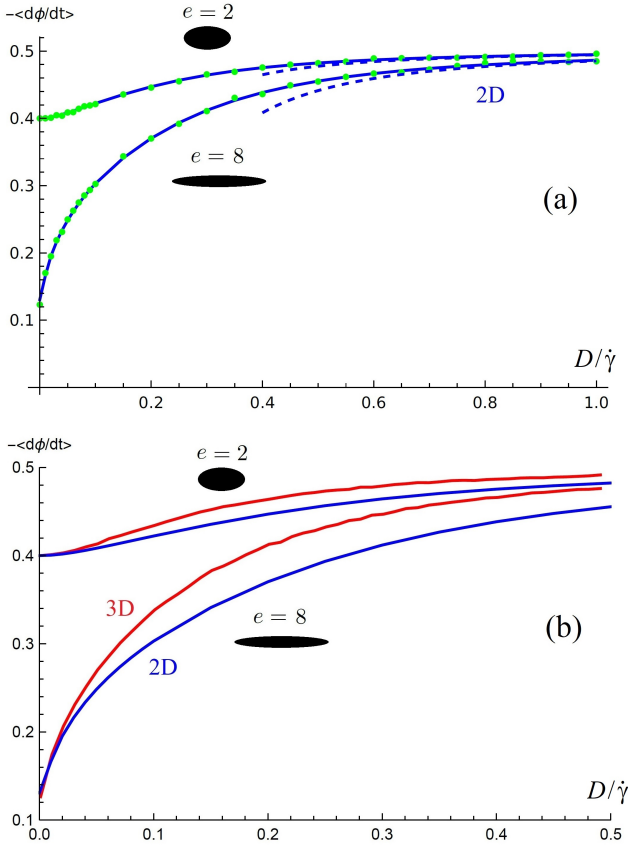


FIG. 12: (a) Mean angular velocity for particle elongations $e = 2, 8$ in two dimensions (2D) from the Fokker-Planck approach (solid lines) and Langevin simulations (points). The limiting values for small D are correctly given by Eq. (63). The dashed curves show the perturbation theory to second order. (b) Comparison of mean angular velocity in 2D and 3D for $e = 2, 8$.

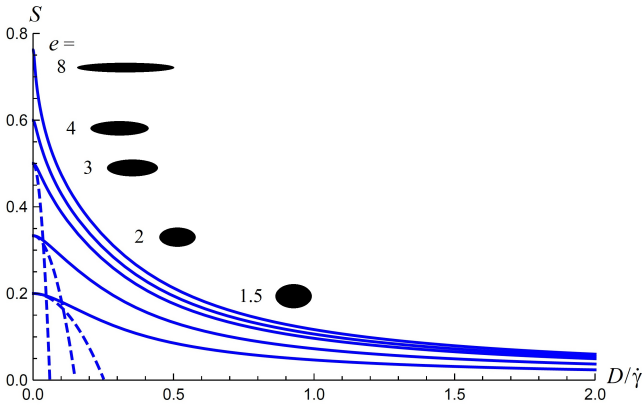


FIG. 13: Nematic order parameter S as a function of the noise for $e = 1.5, 2, 3, 4, 8$, bottom-to-top. The dashed lines show perturbation theory to second order, Eq. (68).

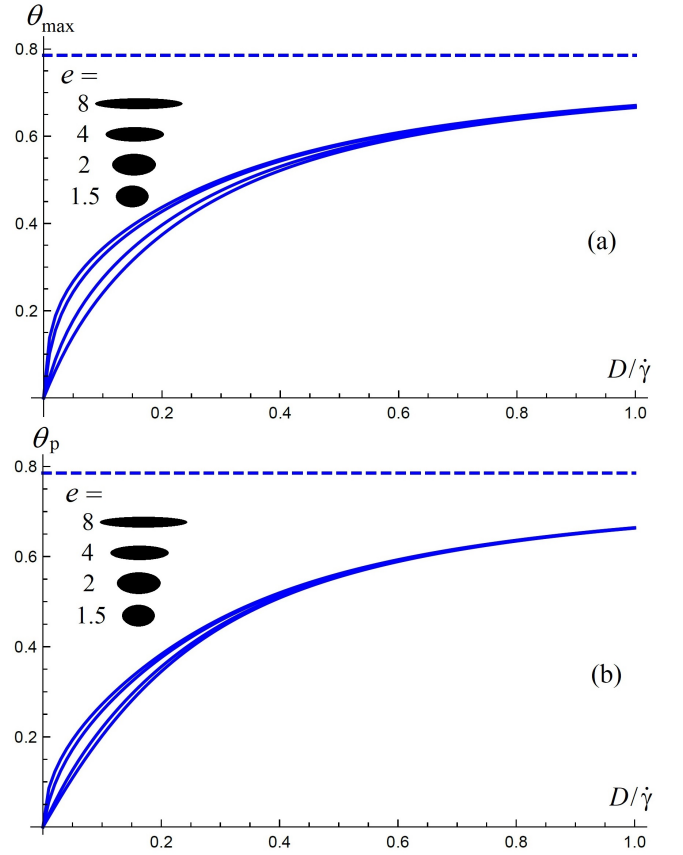


FIG. 14: (a) Angle for which the distribution displays a maximum and (b) θ_p as a function of the noise for $e = 8, 4, 2, 1.5$ top-to-bottom calculated from the exact solution. For large noise, both approach $\pi/4$ (dashed line).

VIII. CONCLUSION

Jeffery orbits with noise can describe a variety of systems with anisometric particles under shear. In this contribution we extended the analytical result of Doi and Edwards for infinitely thin needles to particles with arbitrary shape factor, β . We examined the orientation order matrix as a function of the noise (or inverse Péclet number) and the particle elongation. The solutions of the Fokker-Planck equation agree with numerical simulations of the Langevin equation. Nematic ordering increases monotonically with increasing Péclet number at fixed shape and with increasing orientation at fixed Péclet number. By contrast, the biaxiality obtained for an elongated particle ($\beta > 6$) exhibits a maximum for $Pe \approx 1.2$. We also examined the behavior of the strictly two-dimensional system. Comparing the 2D and 3D data we find larger average rotation speed of the particle in a three-dimensional system for the same noise amplitude.

Systems of sheared inelastic particles under shear flow [49] show alignment. These are typically dense systems

with significant particle-particle interactions. In two-dimensions, it appears that, at least quantitatively, the orientational distribution of a system of inelastic hard dumbbells [45] resembles that of the Jeffery orbit with constant noise. It would be interesting to see if the same applies to the three dimensional systems considered in e.g. [49, 63]. If there are significant differences can these systems be modeled using Jeffery orbits with an orienta-

tion dependent noise?

ACKNOWLEDGMENTS

We acknowledge support from CNRS PICS Grant No. 08187 and the Hungarian Academy of Sciences Grant No. NKM-2018-5. JT thanks V. Kumaran and Hartmut Löwen for helpful discussions.

Appendix A: From Stratonovich to Itô expression of the Langevin equation

The usual Stratonovich expression of the rotational diffusion (without any deterministic part)

$$\text{(Strato)} \quad d\mathbf{p} = \mathbf{B}(\mathbf{p}) \circ \boldsymbol{\xi} dt \quad (\text{A1})$$

with

$$\mathbf{B}(\mathbf{p}) = \sqrt{2D} \begin{pmatrix} 0 & -p_z & p_y \\ p_z & 0 & -p_x \\ -p_y & p_x & 0 \end{pmatrix} \quad (\text{A2})$$

can be turned into an Itô expression with the help of Itô's formula

$$\text{(Itô)} \quad (d\mathbf{p})_i = \sqrt{2D} (\mathbf{p} \times \boldsymbol{\xi})_i dt + \frac{1}{2} \sum_{j,k} B_{kj} \partial_k B_{ij} dt \quad (\text{A3})$$

where the last term (drift induced by the multiplicative noise $\mathbf{B}(\mathbf{p}) \boldsymbol{\xi} dt$) can also be written as $-2Dp_i dt$, giving:

$$\text{(Itô)} \quad \frac{d\mathbf{p}}{dt} = \sqrt{2D} \mathbf{p} \times \boldsymbol{\xi} - 2D\mathbf{p} \quad (\text{A4})$$

Adding the deterministic part (Jeffery orbits equation) does not modify the expression of the drift term $-2D\mathbf{p}$

$$\text{(Strato)} \quad \frac{d\mathbf{p}}{dt} = (\mathbf{I} - \mathbf{p} \otimes \mathbf{p}) (\beta\mathbf{E} + \mathbf{W}) \mathbf{p} + \mathbf{B}(\mathbf{p}) \circ \boldsymbol{\xi} dt \quad (\text{A5})$$

$$\text{(Itô)} \quad \frac{d\mathbf{p}}{dt} = (\mathbf{I} - \mathbf{p} \otimes \mathbf{p}) (\beta\mathbf{E} + \mathbf{W}) \mathbf{p} + \sqrt{2D} \mathbf{p} \times \boldsymbol{\xi} - 2D\mathbf{p} \quad (\text{A6})$$

since the latter arises only from the multiplicative noise term, independently from the deterministic part.

The passage from Cartesian (p_x, p_y, p_z) to spherical (p_r, p_θ, p_ϕ) coordinates is also readily obtained with the help of the Itô's formula for a change of variables (see [64]):

$$\frac{df(\mathbf{p})}{dt} = \nabla f \cdot \mathbf{A} + \nabla f \cdot \mathbf{B}\boldsymbol{\xi} + \frac{1}{2} \sum_{i,j} (BB^\top)_{ij} \partial_i \partial_j f(\mathbf{p}) \quad (\text{A7})$$

for the general case where $\frac{d\mathbf{p}}{dt} = \mathbf{A}(\mathbf{p}) + \mathbf{B}(\mathbf{p}) \boldsymbol{\xi}$.

One gets (without the deterministic part)

$$\frac{d\theta}{dt} = \frac{d}{dt} (\arccos(p_z)) = D \cot(\theta) + \sqrt{2D} [\sin(\phi) \xi_x - \cos(\phi) \xi_y] \quad (\text{A8})$$

$$\frac{d\phi}{dt} = \frac{d}{dt} (\arctan(p_y/p_x)) = \frac{\sqrt{2D}}{\sin(\theta)} [\cos(\theta) (\cos(\phi) \xi_x + \sin(\phi) \xi_y) - \sin(\theta) \xi_z] \quad (\text{A9})$$

We can define three new Brownian motions

$$\xi_1 = \sin(\phi) \xi_x - \cos(\phi) \xi_y \quad (\text{A10})$$

$$\xi_2 = \cos(\theta) (\cos(\phi) \xi_x + \sin(\phi) \xi_y) - \sin(\theta) \xi_z \quad (\text{A11})$$

$$\xi_3 = \sin(\theta) (\cos(\phi) \xi_x + \sin(\phi) \xi_y) + \cos(\theta) \xi_z \quad (\text{A12})$$

as linear combinations of the independent Brownian motions (ξ_x, ξ_y, ξ_z) through an orthogonal matrix $\tilde{\mathbf{S}}$

$$\tilde{\mathbf{S}} = \begin{pmatrix} \sin \phi & -\cos \phi & 0 \\ \cos \theta \cos \phi & \cos \theta \sin \phi & -\sin \theta \\ \sin \theta \cos \phi & \sin \theta \sin \phi & \cos \theta \end{pmatrix} \quad (\text{A13})$$

Then, it is easy to check that they are independent (see [64]) and orthonormal ($\xi_i \cdot \xi_j = \delta_{ij}$ in the $\{\xi_x, \xi_y, \xi_z\}$ basis).

One finally obtains the expressions

$$\frac{d\theta}{dt} = D \cot \theta + \sqrt{2D} \xi_1 \quad (\text{A14})$$

$$\frac{d\phi}{dt} = \frac{\sqrt{2D}}{\sin \theta} \xi_2 \quad (\text{A15})$$

to which the deterministic Jeffery's terms must be added to get Eq. (15-18).

The conservation of the norm of the unit vector \mathbf{p} can also be readily seen using Itô's formula for $f(\mathbf{p}) = \mathbf{p} \cdot \mathbf{p} = p^2$. In this case, the last term of Eq. (A7) becomes

$$\frac{1}{2} \sum_{i,j} (\mathbf{B}\mathbf{B}^\top)_{ij} \partial_i \partial_j f(\mathbf{p}) = 4Dp^2 \quad (\text{A16})$$

compensating exactly the drift induced term $\nabla f \cdot \mathbf{A}$ in Eq. (A7), while the $\nabla f \cdot \mathbf{B}\boldsymbol{\xi}$ term vanishes since

$$\nabla f \cdot \mathbf{B}\boldsymbol{\xi} = -2\sqrt{2D}\mathbf{p} \cdot (\mathbf{p} \times \boldsymbol{\xi}) = 0 \quad (\text{A17})$$

Finally

$$\frac{d(p^2)}{dt} = 2\mathbf{p} \cdot (\mathbf{I} - \mathbf{p} \otimes \mathbf{p}) (\beta\mathbf{E} + \mathbf{W}) \mathbf{p} = 2(1 - p^2) \mathbf{p} \cdot (\beta\mathbf{E} + \mathbf{W}) \mathbf{p} \quad (\text{A18})$$

showing that $\frac{d(p^2)}{dt} = 0$ at any time if $p^2 = 1$ at the initial time.

Appendix B: Computation of the $(lm|\hat{\Lambda}|l'm')$

In this appendix we detail how to compute the $(lm|\hat{\Lambda}|l'm')$ matrix elements necessary for the evaluation of the b_{lm} coefficients of the distribution function $\psi(\theta, \phi)$ appearing in Eq. (29) and evaluated in Eq. (30).

As shown in the main text, the operator $\hat{\Lambda}$ can be written as $\hat{\Lambda} = \beta\hat{\Lambda}_1 + \frac{1-\beta}{2}i\hat{L}_y$ for an elongated particle of shape factor β . The operator $\hat{\Lambda}_1$ introduced by Doi and Edwards in [44] depends on the usual spherical harmonics Y_l^m and angular momentum operators \hat{L}_z and \hat{L}_y .

For the contribution from \hat{L}_z and $i\hat{L}_y$, we use

$$\langle l, m | \hat{L}_z | l', m' \rangle = m \delta_{l,l'} \delta_{m,m'} \quad (\text{B1})$$

and

$$\langle l, m | i\hat{L}_y | l', m' \rangle = \frac{1}{2} \sqrt{l(l+1) - m(m-1)} \delta_{l,l'} \delta_{m-1,m'} - \frac{1}{2} \sqrt{l(l+1) - m(m+1)} \delta_{l,l'} \delta_{m+1,m'} \quad (\text{B2})$$

leading to

$$(l, m | i\hat{L}_y | l', m') = \frac{gm}{2} \left[\sqrt{l(l+1) - m(m-1)} g_{m-1} \delta_{m-1,m'} - \sqrt{l(l+1) - m(m+1)} g_{m+1} \delta_{m+1,m'} \right] \delta_{l,l'} \quad (\text{B3})$$

where $g_0 = \sqrt{2}$, $g_m = 1$ if $m > 0$, and $g_m = 0$ if $m < 0$.

For the terms implying the spherical harmonics in $\hat{\Lambda}_1$, we use the relation

$$\langle l, m | Y_p^q | l', m' \rangle = (-1)^m \sqrt{\frac{(2l+1)(2p+1)(2l'+1)}{4\pi}} \begin{pmatrix} l & p & l' \\ 0 & 0 & 0 \end{pmatrix} \begin{pmatrix} l & p & l' \\ -m & q & m' \end{pmatrix} \quad (\text{B4})$$

in terms of the Wigner 3-j symbols

$$\begin{pmatrix} j_1 & j_2 & j_3 \\ m_1 & m_2 & m_3 \end{pmatrix} = \frac{(-1)^{j_1-j_2-m_3}}{\sqrt{2j_3+1}} \langle j_1, m_1; j_2, m_2 | j_3, m_3 \rangle \quad (\text{B5})$$

which are different from 0 only if $|j_1 - j_2| \leq j_3 \leq j_1 + j_2$, $m_3 = -m_1 - m_2$ and $-j_k \leq m_k \leq j_k$ for $k = 1, 2, 3$.

As noted in [44], only a few $(l, m | \hat{\Lambda}_1 | l', m')$ terms are different from zero in the summation of Eq. (30). These are

$$(l, m | \hat{\Lambda}_1 | l, m - 1) = g_{m-1} G_1(l, m - 1) \quad (\text{B6})$$

$$(l, m | \hat{\Lambda}_1 | l, m + 1) = -g_m G_1(l, -m - 1) \quad (\text{B7})$$

$$(l, m | \hat{\Lambda}_1 | l + 2, m - 1) = g_{m-1} G_2(l, m - 1) \quad (\text{B8})$$

$$(l, m | \hat{\Lambda}_1 | l + 2, m + 1) = -g_m G_2(l, -m - 1) \quad (\text{B9})$$

$$(l, m | \hat{\Lambda}_1 | l - 2, m - 1) = g_{m-1} G_3(l - 2, m - 1) \quad (\text{B10})$$

$$(l, m | \hat{\Lambda}_1 | l - 2, m + 1) = -g_m G_3(l - 2, -m - 1), \quad (\text{B11})$$

where

$$g_m = \begin{cases} \sqrt{2} & \text{if } m = 0 \\ 1 & \text{otherwise} \end{cases} \quad (\text{B12})$$

and

$$G_1(l, m) = \frac{2l^2 + 2l + 3m}{2(2l+1)(2l+3)} [(l-m)(l+m+1)]^{1/2} \quad (\text{B13})$$

$$G_2(l, m) = \frac{l}{2(2l+3)} \left[\frac{(l+m+2)(l-m)(l-m+1)(l-m+2)}{(2l+1)(2l+5)} \right]^{1/2} \quad (\text{B14})$$

$$G_3(l, m) = \frac{l+3}{2(2l+3)} \left[\frac{(l-m+1)(l+m+1)(l+m+2)(l+m+3)}{(2l+1)(2l+5)} \right]^{1/2} \quad (\text{B15})$$

following the notation of Doi and Edwards in [44].

Appendix C: Perturbation theory in 3D using Pe as the expansion parameter

Here we develop a perturbation theory using the Péclet number $Pe = \dot{\gamma}/D$ as the expansion parameter. The Fokker-Planck equation may be written as

$$Pe \Lambda \psi = \nabla^2 \psi \quad (\text{C1})$$

Let us expand the orientational distribution function as a power series in Pe :

$$\psi = \psi_0 + Pe \psi_1 + Pe^2 \psi_2 + \dots \quad (\text{C2})$$

Substituting in the FP equation and equating powers of Pe we obtain at zeroth, first and second order

$$\begin{aligned}\nabla^2\psi_0 &= 0 \\ \Lambda\psi_0 &= \nabla^2\psi_1 \\ \Lambda\psi_1 &= \nabla^2\psi_2\end{aligned}\tag{C3}$$

Solving we find

$$\psi_0 = \frac{1}{4\pi}\tag{C4}$$

$$\psi_1 = -\frac{\beta}{4\pi}\sqrt{\frac{\pi}{15}}|21)\tag{C5}$$

$$\psi_2 = -\frac{(7-\beta)\beta}{336\sqrt{5\pi}}|20) + \frac{(7+3\beta)\beta}{336\sqrt{15\pi}}|22) - \frac{\beta^2}{420\sqrt{\pi}}|40) + \frac{\beta^2}{168\sqrt{5\pi}}|42)\tag{C6}$$

which gives the scalar order parameter

$$s = \frac{1}{15}\beta Pe + O(Pe^2)\tag{C7}$$

Note that for small Pe (or large $D/\dot{\gamma}$) Eq. (D12) reduces to this expression. Similarly we find

$$\langle\cos(2\phi)\rangle = \frac{(5+3\beta)\beta}{720}Pe^2 + O(Pe^3)\tag{C8}$$

Appendix D: Perturbation theory in 3D using β as the expansion parameter

We know that when $\beta = 0$, corresponding to a sphere, the orientational distribution is uniform: $\psi(\theta, \phi) = 1/(4\pi)$. This prompts us to try a perturbation approach. Let

$$\psi(\beta, \theta, \phi) = \psi_0(\theta, \phi) + \beta\psi_1(\theta, \phi) + \beta^2\psi_2(\theta, \phi) + \dots\tag{D1}$$

Substituting in the Langevin equation gives

$$\left[\beta\hat{\Lambda}_1 + \frac{1-\beta}{2}i\hat{L}_y\right]\psi(\beta, \theta, \phi) = \epsilon\nabla^2\psi(\beta, \theta, \phi)\tag{D2}$$

where $\epsilon = D/\dot{\gamma}$. Expanding in β and equating the coefficients of equal powers gives

$$\frac{1}{2}i\hat{L}_y\psi_0 = \epsilon\nabla^2\psi_0\tag{D3}$$

$$\Lambda_1\psi_0 + \frac{1}{2}i\hat{L}_y(\psi_1 - \psi_0) = \epsilon\nabla^2\psi_1\tag{D4}$$

Clearly $\psi_0 = 1/4\pi$ and the second equation becomes

$$3\sqrt{\frac{4\pi}{15}}\frac{S_2^1}{4\pi} + \frac{1}{2}i\hat{L}_y\psi_1 = \epsilon\nabla^2\psi_1\tag{D5}$$

Let us assume

$$\psi_1 = b_{20}|20) + b_{21}|21) + b_{22}|22)\tag{D6}$$

Substituting in the above equation and using the orthonormality of the functions $|lm)$ we find

$$3\sqrt{\frac{4\pi}{15}}\frac{1}{4\pi} + \frac{\sqrt{3}}{2}b_{20} - \frac{1}{2}b_{22} = -6\epsilon b_{21}\tag{D7}$$

$$-\frac{\sqrt{3}}{2}b_{21} = -6\epsilon b_{20}\tag{D8}$$

$$\frac{1}{2}b_{21} = -6\epsilon b_{22}\tag{D9}$$

Solving these equations and using the coefficients to evaluate the order matrix we find

$$\mathbf{Q} = \begin{pmatrix} \frac{\beta}{5\sqrt{1+36\epsilon^2}} & 0 & \frac{6(\epsilon)\beta}{5\sqrt{1+36\epsilon^2}} \\ 0 & 0 & 0 \\ \frac{6(\epsilon)\beta}{5\sqrt{1+36\epsilon^2}} & 0 & -\frac{\beta}{5\sqrt{1+36\epsilon^2}} \end{pmatrix} \quad (\text{D10})$$

The eigenvalues are

$$\left(\frac{\beta}{5\sqrt{36\epsilon^2+1}}, 0, \frac{-\beta}{5\sqrt{36\epsilon^2+1}} \right) \quad (\text{D11})$$

and hence we find the scalar order parameters

$$s = 2r = \frac{2\beta}{5\sqrt{1+36\epsilon^2}} \quad (\text{D12})$$

Appendix E: The scalar order parameters s and r for Jeffery orbits with a random initial orientation

For a given initial orientation specified by ϕ_0, θ_0 the corresponding values of the parameters C and κ are given by

$$C^2 = \tan^2(\theta_0)(e^2 \sin^2 \phi_0 + \cos^2 \phi_0)/e^2 \quad (\text{E1})$$

$$\kappa = \arctan(e \tan(\phi_0)) \quad (\text{E2})$$

We can calculate the order matrix Eq. (34) by replacing the average over the orientational probability distribution by a time average over one period (actually symmetry allows us to limit this to one quarter period). We then average Q over a sample of random initial orientations and then finally calculate s and r using the procedure given in the main text.

However, a more efficient method is to determine the distribution of $y = C^2$. Assuming a uniform, random orientation we obtain the probability density function

$$f(y) = \frac{e}{\pi(1+e^2y)\sqrt{1+y}} E \left(-\sqrt{\frac{(e^2-1)y}{1+y}} \right), \quad 0 \leq y < \infty \quad (\text{E3})$$

where $E(x)$ is the complete elliptic integral of the second kind. By integrating over one quarter period of the Jeffery orbit we can calculate the order matrix. The non-zero elements are

$$\langle \cos^2 \theta \rangle = \frac{1}{\sqrt{(1+y)(1+e^2y)}} \quad (\text{E4})$$

$$\langle \cos^2 \theta \sin^2 \phi \rangle = \frac{e^2 y}{1+e^2 y + \sqrt{(1+y)(1+e^2y)}} \quad (\text{E5})$$

$$\langle \sin^2 \theta \sin^2 \phi \rangle = \frac{y}{1+y + \sqrt{(1+y)(1+e^2y)}} \quad (\text{E6})$$

We now average these matrix elements over the distribution of $y = C^2$ by multiplying them by $f(y)$ and integrating over the domain. It does not seem possible to obtain analytical expressions for the integrals, but they can be easily evaluated numerically. The order matrix constructed with these elements is diagonal. Evaluating s and r we obtain the results shown in Fig. 8. We note that nematic ordering increases more and more rapidly as β approaches one, while biaxiality displays a maximum value of 0.121 for $\beta = 0.876$ before falling rapidly to zero.

[1] G. B. Jeffery, The motion of ellipsoidal particles immersed in a viscous fluid, Proceedings of the Royal Soci-

ety of London. Series A, Containing papers of a mathematical and physical character **102**, 161 (1922).

- [2] T. Börzsönyi, B. Szabó, S. Wegner, K. Harth, J. Török, E. Somfai, T. Bien, and R. Stannarius, Shear-induced alignment and dynamics of elongated granular particles, *Physical Review E* **86**, 051304 (2012).
- [3] E. Azéma and F. Radjai, Force chains and contact network topology in sheared packings of elongated particles, *Physical Review E* **85**, 031303 (2012).
- [4] M. Boton, E. Azéma, N. Estrada, F. Radjai, and A. Lizcano, Quasistatic rheology and microstructural description of sheared granular materials composed of platy particles, *Physical Review E* **87**, 032206 (2013).
- [5] F. Tapia, S. Shaikh, J. E. Butler, O. Pouliquen, and É. Guazzelli, Rheology of concentrated suspensions of non-colloidal rigid fibres, *Journal of Fluid Mechanics* **827**, R5 (2017).
- [6] D. B. Nagy, P. Claudin, T. Börzsönyi, and E. Somfai, Rheology of dense granular flows for elongated particles, *Physical Review E* **96**, 062903 (2017).
- [7] É. Guazzelli and O. Pouliquen, Rheology of dense granular suspensions, *Journal of Fluid Mechanics* **852**, P1 (2018).
- [8] J. E. Butler and B. Snook, Microstructural dynamics and rheology of suspensions of rigid fibers, *Annual Review of Fluid Mechanics* **50**, 299 (2018).
- [9] M. Trulsson, Rheology and shear jamming of frictional ellipses, *Journal of Fluid Mechanics* **849**, 718 (2018).
- [10] S. N. Bounoua, P. Kuzhir, and E. Lemaire, Shear reversal experiments on concentrated rigid fiber suspensions, *Journal of Rheology* **63**, 785 (2019).
- [11] D. B. Nagy, P. Claudin, T. Börzsönyi, and E. Somfai, Flow and rheology of frictional elongated grains, *New Journal of Physics* **22**, 073008 (2020).
- [12] T. A. Marschall and S. Teitel, Shear-driven flow of athermal, frictionless, spherocylinder suspensions in two dimensions: Stress, jamming, and contacts, *Physical Review E* **100**, 032906 (2019).
- [13] T. A. Marschall, D. Van Hoesen, and S. Teitel, Shear-driven flow of athermal, frictionless, spherocylinder suspensions in two dimensions: Particle rotations and orientational ordering, *Physical Review E* **101**, 032901 (2020).
- [14] M. Khan, R. V. More, A. A. Banaei, L. Brandt, and A. M. Ardekani, Rheology of concentrated fiber suspensions with a load-dependent friction coefficient, *Physical Review Fluids* **8**, 044301 (2023).
- [15] A. Zöttl, K. E. Klop, A. K. Balin, Y. Gao, J. M. Yeomans, and D. G. Aarts, Dynamics of individual Brownian rods in a microchannel flow, *Soft Matter* **15**, 5810 (2019).
- [16] T. Tohme, P. Magaud, and L. Baldas, Transport of non-spherical particles in square microchannel flows: A review, *Micromachines* **12**, 277 (2021).
- [17] J. Einarsson, B. Mihiretie, A. Laas, S. Ankardal, J. Angilella, D. Hanstorp, and B. Mehlig, Tumbling of asymmetric microrods in a microchannel flow, *Physics of Fluids* **28** (2016).
- [18] D. Cordasco and P. Bagchi, Dynamics of red blood cells in oscillating shear flow, *Journal of Fluid Mechanics* **800**, 484 (2016).
- [19] G. Junot, N. Figueroa-Morales, T. Darnige, A. Lindner, R. Soto, H. Auradou, and E. Clément, Swimming bacteria in Poiseuille flow: The quest for active Bretherton-Jeffery trajectories, *Europhysics Letters* **126**, 44003 (2019).
- [20] T. Kaya and H. Koser, Characterization of hydrodynamic surface interactions of *Escherichia coli* cell bodies in shear flow, *Physical Review Letters* **103**, 138103 (2009).
- [21] A. Ganesh, C. Douarche, M. Dentz, and H. Auradou, Numerical modeling of dispersion of swimming bacteria in a Poiseuille flow, *Physical Review Fluids* **8**, 034501 (2023).
- [22] S. A. Berman and K. A. Mitchell, Swimmer dynamics in externally driven fluid flows: The role of noise, *Physical Review Fluids* **7**, 014501 (2022).
- [23] M. Guzmán and R. Soto, Nonideal rheology of semidilute bacterial suspensions, *Physical Review E* **99**, 012613 (2019).
- [24] D. Saintillan, Extensional rheology of active suspensions, *Physical Review E* **81**, 056307 (2010).
- [25] A. Zöttl and H. Stark, Periodic and quasiperiodic motion of an elongated microswimmer in Poiseuille flow, *The European Physical Journal E* **36**, 1 (2013).
- [26] K. Ishimoto, Jeffery's orbits and microswimmers in flows: A theoretical review, *Journal of the Physical Society of Japan* **92**, 062001 (2023).
- [27] F. M. Ventrella, N. Pujara, G. Boffetta, M. Cencini, J.-L. Thiffeault, and F. De Lillo, Microswimmer trapping in surface waves with shear, *arXiv preprint arXiv:2304.14028* (2023).
- [28] F. P. Bretherton, The motion of rigid particles in a shear flow at low Reynolds number, *Journal of Fluid Mechanics* **14**, 284 (1962).
- [29] A. Yarin, O. Gottlieb, and I. Roisman, Chaotic rotation of triaxial ellipsoids in simple shear flow, *Journal of Fluid Mechanics* **340**, 83 (1997).
- [30] F. Lundell, The effect of particle inertia on triaxial ellipsoids in creeping shear: From drift toward chaos to a single periodic solution, *Physics of Fluids* **23** (2011).
- [31] G. Almondo, J. Einarsson, J. Angilella, and B. Mehlig, Intrinsic viscosity of a suspension of weakly Brownian ellipsoids in shear, *Physical Review Fluids* **3**, 064307 (2018).
- [32] S. B. Chen and D. L. Koch, Rheology of dilute suspensions of charged fibers, *Physics of Fluids* **8**, 2792 (1996).
- [33] D. Crowdy, Flipping and scooping of curved 2d rigid fibers in simple shear: The Jeffery equations, *Physics of Fluids* **28** (2016).
- [34] B. D. Leahy, D. L. Koch, and I. Cohen, The effect of shear flow on the rotational diffusion of a single axisymmetric particle, *Journal of Fluid Mechanics* **772**, 42 (2015).
- [35] Z. Yu, N. Phan-Thien, and R. I. Tanner, Rotation of a spheroid in a Couette flow at moderate Reynolds numbers, *Physical Review E* **76**, 026310 (2007).
- [36] F. Lundell and A. Carlsson, Heavy ellipsoids in creeping shear flow: Transitions of the particle rotation rate and orbit shape, *Physical Review E* **81**, 016323 (2010).
- [37] S. A. Abtahi and G. J. Elfring, Jeffery orbits in shear-thinning fluids, *Physics of Fluids* **31**, 103106 (2019).
- [38] M. Junk and R. Illner, A new derivation of Jeffery's equation, *Journal of Mathematical Fluid Mechanics* **9**, 455 (2007).
- [39] P. Boeder, Über strömungsdoppelbrechung, *Zeitschrift für Physik* **75**, 258 (1932).
- [40] A. Peterlin, Über die viskosität von verdünnten lösungen und suspensionen in abhängigkeit von der teilchenform, *Zeitschrift für Physik* **111**, 232 (1938).
- [41] J. M. Burgers, On the motion of small particles of elongated form suspended in a viscous liquid, *Kon. Ned. Akad. Wet. Verhand.(Eerste Sectie)* **16**, 113 (1938).
- [42] E. Hinch and L. Leal, The effect of Brownian motion on

- the rheological properties of a suspension of non-spherical particles, *Journal of Fluid Mechanics* **52**, 683 (1972).
- [43] L. Leal and E. Hinch, The effect of weak Brownian rotations on particles in shear flow, *Journal of Fluid Mechanics* **46**, 685 (1971).
- [44] M. Doi and S. F. Edwards, Dynamics of rod-like macromolecules in concentrated solution. part 2, *Journal of the Chemical Society, Faraday Transactions 2: Molecular and Chemical Physics* **74**, 918 (1978).
- [45] K. A. Reddy, V. Kumaran, and J. Talbot, Orientational ordering in sheared inelastic dumbbells, *Physical Review E* **80**, 031304 (2009).
- [46] J. K. Dhont and W. J. Briels, Rod-like Brownian particles in shear flow, *Soft Matter: Complex Colloidal Suspensions*, edited by G. Gompper, M. Schick **2** (2006).
- [47] G. Tegze, F. Podmaniczky, E. Somfai, T. Börzsönyi, and L. Gránásy, Orientational order in dense suspensions of elliptical particles in the non-Stokesian regime, *Soft Matter* **16**, 8925 (2020).
- [48] C. S. Campbell, Elastic granular flows of ellipsoidal particles, *Physics of Fluids* **23** (2011).
- [49] T. Börzsönyi, B. Szabó, G. Törös, S. Wegner, J. Török, E. Somfai, T. Bien, and R. Stannarius, Orientational order and alignment of elongated particles induced by shear, *Physical Review Letters* **108**, 228302 (2012).
- [50] A. Pol, R. Artoni, P. Richard, P. R. N. Conceicao, and F. Gabrieli, Kinematics and shear-induced alignment in confined granular flows of elongated particles, *New Journal of Physics* **24**, 073018 (2022).
- [51] F. Perrin, Mouvement brownien d'un ellipsoïde - I. dispersion diélectrique pour des molécules ellipsoïdales, *Journal de Physique et Le Radium* **5**, 497 (1934).
- [52] L. D. Favro, Theory of the rotational Brownian motion of a free rigid body, *Physical Review* **119**, 53 (1960).
- [53] P. S. Hubbard, Rotational Brownian motion, *Physical Review A* **6**, 2421 (1972).
- [54] R. E. D. McClung, The Fokker–Planck–Langevin model for rotational Brownian motion. I. General theory, *The Journal of Chemical Physics* **73**, 2435 (1980).
- [55] J. R. McConnell, *Rotational Brownian motion and dielectric theory* (New York - London: Academic Press, 1980).
- [56] W. Coffey, Y. Kalmykov, and J. Waldron, *The Langevin Equation* (Singapore: World Scientific, 1996).
- [57] W. T. Coffey, Y. P. Kalmykov, and S. V. Titov, Langevin equation method for the rotational Brownian motion and orientational relaxation in liquids: II. symmetrical top molecules, *Journal of Physics A: Mathematical and General* **36**, 4947 (2003).
- [58] D. R. Brillinger, A particle migrating randomly on a sphere, *Journal of Theoretical Probability* **10**, 429 (1997).
- [59] M. Raible and A. Engel, Langevin equation for the rotation of a magnetic particle, *Applied Organometallic Chemistry* **18**, 536 (2004).
- [60] A. Majumdar, Equilibrium order parameters of nematic liquid crystals in the Landau-de Gennes theory, *European Journal of Applied Mathematics* **21**, 181 (2010).
- [61] A. Majumdar and A. Zarnescu, Landau–de Gennes theory of nematic liquid crystals: the Oseen–Frank limit and beyond., *Archive for Rational Mechanics and Analysis* **196**, 227 (2010).
- [62] M. Lettinga and J. Dhont, Non-equilibrium phase behaviour of rod-like viruses under shear flow, *Journal of Physics: Condensed Matter* **16**, S3929 (2004).
- [63] X.-F. Yuan and M. P. Allen, Non-linear responses of the hard-spheroid fluid under shear flow, *Physica A: Statistical Mechanics and its Applications* **240**, 145 (1997).
- [64] C. W. Gardiner, *Handbook of Stochastic Methods for Physics, Chemistry and the Natural Sciences*, 3rd ed., Springer Series in Synergetics (Springer Berlin, 2004).